JOURNAL OF GEOPHYSICAL RESEARCH: PLANETS, VOL. 118, 26–36, doi:10.1029/2012JE004172, 2013

Craters hosting radar-bright deposits in Mercury's north polar region: Areas of persistent shadow determined from MESSENGER images

Nancy L. Chabot,[1] Carolyn M. Ernst,[1] John K. Harmon,[2] Scott L. Murchie,[1] Sean C. Solomon,[3,4] David T. Blewett,[1] and Brett W. Denevi[1]

Received 27 June 2012; revised 24 September 2012; accepted 1 November 2012; published 26 January 2013.

[1] Radar-bright features near Mercury's poles were discovered in Earth-based radar images and proposed to be water ice present in permanently shadowed areas. Images from MESSENGER's one-year primary orbital mission provide the first nearly complete view of Mercury's north polar region, as well as multiple images of the surface under a range of illumination conditions. We find that radar-bright features near Mercury's north pole are associated with locations persistently shadowed in MESSENGER images. Within 10° of the pole, almost all craters larger than 10 km in diameter host radar-bright deposits. There are several craters located near Mercury's north pole with sufficiently large diameters to enable long-lived water ice to be thermally stable at the surface within regions of permanent shadow. Craters located farther south also host radar-bright deposits and show a preference for cold-pole longitudes; thermal models suggest that a thin insulating layer is required to cover these deposits if the radar-bright material consists predominantly of long-lived water ice. Many small (<10 km diameter) and low-latitude (extending southward to 66°N) craters host radar-bright material, and water ice may not be thermally stable in these craters for ~1 Gy, even beneath an insulating layer. The correlation of radar-bright features with persistently shadowed areas is consistent with the deposits being composed of water ice, and future thermal modeling of small and low-latitude craters has the potential to further constrain the nature, source, and timing of emplacement of the radar-bright material.

Citation: Chabot, N. L., C. M. Ernst, J. K. Harmon, S. L. Murchie, S. C. Solomon, D. T. Blewett, and B. W. Denevi (2013), Craters hosting radar-bright deposits in Mercury's north polar region: Areas of persistent shadow determined from MESSENGER images, *J. Geophys. Res. Planets*, *118*, 26–36, doi:10.1029/2012JE004172.

1. Introduction

[2] From radar images of Mercury acquired by the 70 m antenna in Goldstone, California, and the Very Large Array, a radar-bright feature was first discovered surrounding the planet's north pole [*Slade et al*., 1992; *Butler et al*., 1993]. Observations made from the Arecibo Observatory quickly confirmed the north polar radar-bright feature and also documented similar radar-bright material in Mercury's south polar region [*Harmon and Slade*, 1992]. The high reflectivity and high circular polarization ratio, the ratio of reflected power in the same sense of circular polarization as that transmitted to the reflected power in the opposite sense of polarization, of the observed features are distinguishing traits also seen on the icy Galilean satellites of Jupiter and at the Martian south polar ice cap, and the radar observations were interpreted to be evidence of water ice in Mercury's polar regions. Mercury's obliquity is only 2.04 arc minutes (0.034°) [*Margot et al*., 2012], so the interiors of some craters and other topographic depressions near the poles do not receive any direct sunlight. Early thermal modeling calculations indicated that water ice potentially could be stable within permanently shadowed craters at Mercury's poles for billions of years [*Paige et al*., 1992].

[3] Over the subsequent two decades, further Earth-based observations greatly improved the spatial resolution of the radar data. Many individual radar-bright spots were identified, and some were mapped to the interiors of impact craters, consistent with the original proposal of water ice on the permanently shadowed floors of high-latitude craters [*Harmon et al*., 1994, 2001, 2011; *Slade et al*., 2001; *Harcke*, 2005; *Harmon*, 2007]. However, the association with craters or other geologic features could not be established where

[1]The Johns Hopkins University Applied Physics Laboratory, Laurel, Maryland, USA.
[2]National Astronomy and Ionosphere Center, Arecibo Observatory, Arecibo, Puerto Rico, USA.
[3]Department of Terrestrial Magnetism, Carnegie Institution of Washington, Washington, DC, USA.
[4]Lamont-Doherty Earth Observatory, Columbia University, Palisades, New York, USA.

Corresponding author: N. L. Chabot, The Johns Hopkins University Applied Physics Laboratory, Laurel, MD, 20723, USA. (nancy.chabot@jhuapl.edu)

2169-9097/12/2012JE004172

visible-image coverage by spacecraft was absent. Two encounters by Mariner 10 in 1974–1975 provided coverage of slightly less than half of Mercury's polar regions [*Davies et al*., 1978], and the three Mercury flybys by the MErcury Surface, Space ENvironment, GEochemistry, and Ranging (MESSENGER) spacecraft in 2008–2009 were along near-equatorial trajectories and did not provide new data of terrain at high latitudes [*Solomon et al*., 2007].

[4] With the improved spatial resolution of the radar data, small radar-bright features were discovered at lower latitudes (more than 10° in latitude from the poles) and in association with small craters (<10 km in diameter) [*Harmon et al*., 2001, 2011; *Harcke*, 2005; *Harmon*, 2007]. Thermal models of permanently shadowed craters on Mercury showed that the presence of radar-bright material in these low-latitude or small-diameter craters is consistent with water ice that is stable for a billion years only if coverage by a thin regolith layer provides thermal insulation for the deposit [*Vasavada et al*., 1999], and even under that condition attributing some of the deposits in small craters to long-lived water ice poses a challenge [*Harmon et al*., 2001]. Alternatives to the water-ice hypothesis have been suggested, including that the radar-bright features on Mercury result from volume scattering in deposits of elemental sulfur [*Sprague et al*., 1995] or from low dielectric loss in silicates at extremely low temperatures [*Starukhina*, 2001].

[5] On 18 March 2011, MESSENGER became the first spacecraft to orbit the planet Mercury, and during the one-year primary orbital mission, MESSENGER's Mercury Dual Imaging System (MDIS) [*Hawkins et al*., 2007] returned 88,746 images from Mercury orbit. One of the early MDIS campaigns, carried out during the first Mercury solar day of the mission's science phase, imaged the south polar region repeatedly. Results of that campaign indicated that all radar-bright features near Mercury's south pole are located in areas of permanent shadow [*Chabot et al*., 2012]. The MESSENGER spacecraft's orbit is highly eccentric, with a minimum altitude of ~200–500 km in the north and a maximum altitude of ~15,200 km in the south during the primary mission. This eccentric orbit did not allow a comparable campaign of regularly repeated images for Mercury's north polar region, because of the substantially smaller image footprint, the need to balance the imaging and data volume needs of other MDIS imaging campaigns, and the competing requirements for low-altitude measurements by other MESSENGER investigations. However, the global imaging campaigns completed by MDIS during the primary mission still provided multiple views of the surface near Mercury's north pole. From those images, we have identified areas in persistent shadow in Mercury's north polar region. In this paper, we compare the spatial distribution of shadowed areas with the locations of radar-bright deposits identified by Earth-based radar observations, and we discuss the implications for the nature of the radar-bright material at Mercury's polar regions and the hypothesis that it consists predominantly of water ice.

2. Method

[6] Images acquired during MESSENGER's one-year primary orbital mission provided near-global coverage of Mercury's surface up to ~86°N. Additionally, three distinct global imaging campaigns were completed during this time: a monochrome base map acquired at low emission angle with >99% coverage at ~200 m/pixel, a complementary stereo-pair map with >92% coverage at ~200 m/pixel, and an 8-color map with >99% coverage at ~900 m/pixel. In the northern hemisphere, MDIS's wide-angle camera (WAC), and the 750-nm narrow-band color filter in particular, was used for all three of these global campaigns, with different levels of pixel binning resulting in different resolutions for the monochrome and color base maps. Major MDIS imaging campaigns during MESSENGER's primary mission were focused largely on global mapping of the planet. MDIS also has a narrow-angle camera (NAC) that was used in the northern hemisphere to acquire high-resolution targeted images at ~50 m/pixel or better. Only ~4% of the planet was covered by high-resolution NAC images during MESSENGER's primary mission. Inspection of the NAC images located north of 65°N showed only minor coverage in comparison with the WAC data set obtained by the major global mapping campaigns, and consequently we chose to use only WAC images for this study. A mosaic of Mariner 10 images [*Robinson et al*., 1999] was also examined but not used; it provided only minimal additional coverage and showed considerable differences in registration from MESSENGER's orbital images within 5° of the pole.

[7] Images for the stereo base map were acquired approximately one Mercury solar day after the corresponding paired images in the monochrome base map, with a similar illumination but different viewing geometry. In contrast, the monochrome and color base map images were acquired during different local times during a Mercury solar day and provide a view of Mercury's surface under different illumination conditions. Figure 1 illustrates this point for a region in Mercury's north polar region near 80°N, 120°E. Under the different illumination conditions, the locations of the shadows change. By using these two views, areas that are shadowed in both can be identified.

[8] In total, 6566 WAC 750-nm-filter images were acquired with image centers at latitudes ≥65°N during MESSENGER's primary orbital mission from 18 March 2011 to 17 March 2012, as shown in Figure 2. Figure 2a shows that the majority of Mercury's surface in the northern region was imaged multiple times during the primary mission, though small areas of Mercury's surface north of 86°N were not imaged at all. The high number of images is a result of ensuring that the three global imaging campaigns each contained overlap between neighboring images and that each was free of small gaps. However, imaging the same surface region a large number of times does not necessarily provide new information about shadowed areas, especially as image overlap often occurs for images acquired during a similar period of time and as the monochrome and stereo base maps were designed to be acquired under similar lighting conditions. For this study, Figures 2b and 2c provide a more relevant look at the available data by examining the range of solar incidence angles under which each portion of the surface was imaged. That the minimum incidence angle shown in Figure 2b differs markedly from the maximum incidence angle shown in Figure 2c indicates that this northern WAC 750-nm-filter data set provides views of Mercury's surface under a wide range of illumination conditions, as is needed for the mapping of locations of persistent shadow.

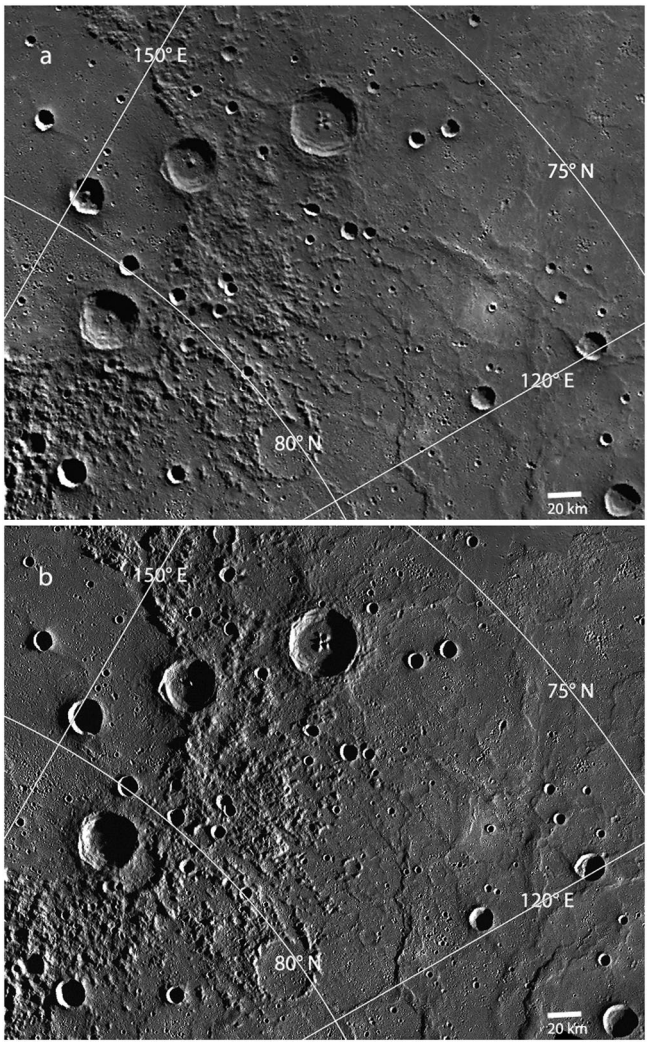

Figure 1. An example of WAC image mosaics of the same surface acquired under different illumination conditions, illustrating the different locations of areas of shadow. Images with varying illumination were used to identify the regions of Mercury's north polar region in persistent shadow in all images from MESSENGER's primary orbital mission.

Additionally, the minimum incidence angle shown in Figure 2 is nearly equal to the latitude in most areas, corresponding to imaging near local noon when shadows are minimized.

[9] Each of the 6566 images was divided into shadowed and sunlit areas, in a manner similar to that done for the Moon [*Bussey et al*., 1999, 2005; *Speyerer and Robinson*, 2011] and Mercury's south polar region [*Chabot et al*., 2012]. For images south of 84°N, a photometric correction was first applied to the images prior to thresholding into sunlit and dark regions to account for differences in viewing and lighting conditions. The photometric correction did not work well at the extreme incidence and phase angles for images located at 84°N and northward and resulted in loss of image coverage for the area nearest to the north pole. Thus, for images located at 84°N and northward, thresholding into sunlit and shadowed areas was conducted with no initial photometric correction. Different threshold values were explored and resulted in the extent of shadowed regions varying by ~25%, similar to results seen in a study of Mercury's south polar region [*Chabot et al*., 2012], but no change in the general locations of shadowing.

[10] Regions determined to be in shadow in Mercury's north polar region in all of the WAC 750-nm-filter images acquired during MESSENGER's primary mission are shown in Figure 3. The incomplete mapping northward of ~86°N complicates the calculation of total shadowed area, as a high percentage of shadowed terrain is located within 5° of the pole. For the region between 65°N and 85°N, ~1% of the surface is shadowed in all images from the primary mission; for the region between 80°N to 85°N, the percentage increases to ~3%. This percentage value is similar to that reported for the same latitude range for areas of permanent shadow at Mercury's south polar region (~2.8%) [*Chabot et al*., 2012] and areas of permanent shadow in the Moon's north (3.8%) and south (4.2%) polar regions [*Mazarico et al*., 2011]. Whereas the studies of *Chabot et al*. [2012] and *Mazarico et al*. [2011] determined areas of permanent shadow, in this work we are able only to identify those areas that were persistently in shadow in all images from MESSENGER's primary mission.

3. Results and Implications

3.1. Mapping Craters That Host Radar-Bright Deposits

[11] The highest-resolution radar image of Mercury's north polar region [*Harmon et al*., 2011], with a range resolution of 1.5 km, is the basis for our comparison with MDIS images. Figure 4a overlays the *Harmon et al*. [2011] radar image on an uncontrolled MESSENGER mosaic of Mercury's north polar region created from images from MESSENGER's primary mission. The *Harmon et al*. [2011] radar image was assembled from Arecibo observations obtained at S-band (12.6-cm wavelength) from 1999–2005 and is a sum of multiple images with the same sense of circular polarization as that transmitted. Figure 4a shows qualitatively that there is extremely good agreement between the radar-bright deposits and the interiors of impact craters.

[12] The map of persistently shadowed areas in Figure 3 is shown together with the image of radar-bright deposits from *Harmon et al*. [2011] in Figure 4b. A quantitative comparison of the shadow map and a median-filtered radar image indicates that ~70% of the radar-bright features between 65°N and 85°N, excluding more northern latitudes where MDIS imaging is incomplete, correspond to areas mapped as persistently shadowed. The remaining ~30% of features are located within ~4 km of areas mapped as persistently shadowed or appear to map to the interiors of small craters. The accuracy of the radar positions is reported to be about 2 km [*Harmon et al*., 2011]. Comparisons of uncontrolled and controlled MDIS mosaics [*Becker et al*., 2012] show that the average offset for ~3000 images located north of 65°N is ~400 m, with a maximum offset of ~1.8 km. The MDIS pixel registration uncertainty also has an effect on the areas that are mapped as persistently shadowed, because such a location must be shadowed in all available images. Any misregistration between the images will result in misregistration of the shadowed areas and will have the effect of decreasing the area mapped as shadowed. As shown in

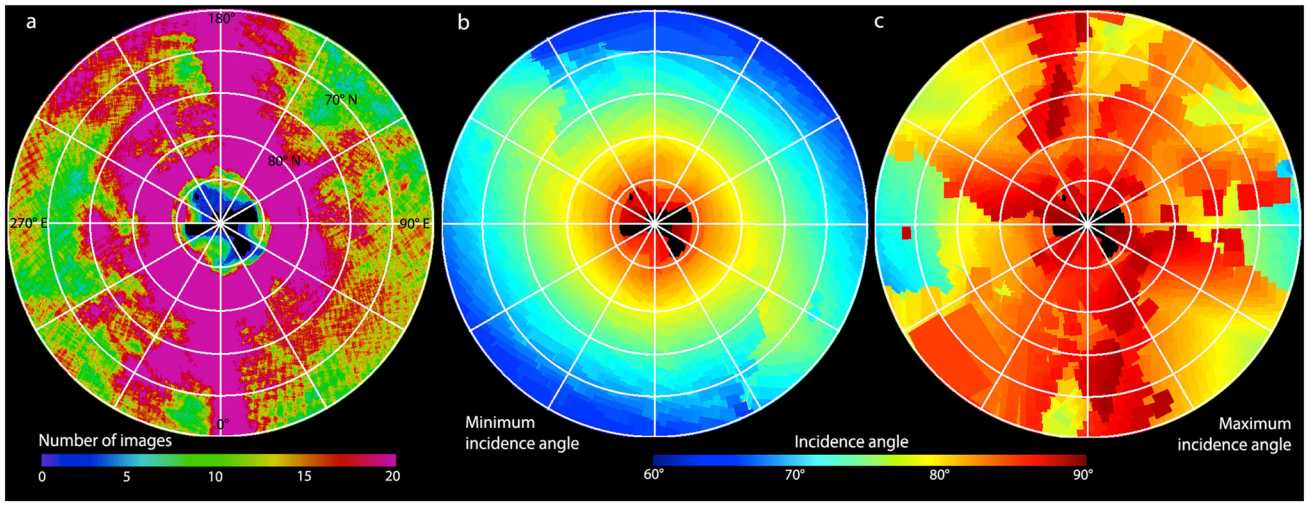

Figure 2. Overview of WAC 750-nm-filter images centered at latitudes ≥65°N acquired during MESSENGER's one-year primary orbital mission. (a) Number of images. The majority of the north polar surface was imaged more than 10 times. (b) Minimum incidence angle. The minimum incidence angle under which a surface was imaged is correlated with the latitude, indicating that the surface was imaged under the conditions expected to cast the least shadows. (c) Maximum incidence angle. The maximum incidence angle differs considerably from the minimum, illustrating that the surface was viewed under a range of illumination conditions.

Figure 2a, the majority of the north polar region was covered by 10 or more images, adding to the potential for image misregistration to yield underestimates of the size of each shadowed area. Similarly, shadowed areas less than ~1 km in horizontal extent are not likely to be identified due to these limitations on uncontrolled image registration. Generally, all large radar-bright deposits collocate with or are located within a few kilometers of areas mapped as persistently shadowed, a result consistent with the uncertainties in the coregistration of the two data sets and the effects of misregistration on sizes of locations mapped as persistently shadowed.

[13] The locations of 305 craters ≥10 km in diameter identified as containing in their interiors some amount of persistently shadowed area are shown in map view in Figure 5a. Mapping was limited to craters, which are the source of the large majority of shadow locations, although ridges and other topographic features are also infrequent sites of persistent shadow as well as radar-bright deposits. The ridge located near 83°N, 270°E, is a good example of a feature other than a crater casting a shadow and hosting radar-bright material. Mapping was limited to craters ≥10 km in diameter because of the MDIS misregistration effects and resolution of the radar data. Mapping is incomplete north of ~86°N, where MDIS image coverage is limited or lacking. Of the 305 shadowed craters mapped, 92 also host radar-bright deposits.

[14] The distribution of these craters by diameter and central latitude is shown in Figure 5b. As seen in both parts of Figure 5, nearly all craters within 10° of Mercury's north pole that have persistently shadowed regions also host radar-bright deposits. Most of the exceptions, craters within 10° of the pole with persistent shadow but without radar-bright material, have diameters <20 km. Overall, this finding that nearly all persistently shadowed craters within 10° of the north pole host radar-bright deposits is similar but not identical to the results for Mercury's south pole [*Chabot et al*., 2012]. In the south, the large majority of permanently shadowed regions within 10° of the pole also host radar-bright deposits, but there are some exceptions, notably near 0°E longitude. The Arecibo Earth-based radar observations of Mercury's south polar region, however, are more limited than those for Mercury's north polar region [*Harmon et al*., 2011]. The nearly 100% agreement between persistently shadowed craters and radar-bright areas within 10° of Mercury's north pole may suggest that a similar result will hold for Mercury's south polar region once additional radar images at different viewing geometries are obtained.

[15] In contrast to the nearly complete correspondence of persistently shadowed locations and craters hosting radar-bright deposits within 10° of Mercury's north pole, craters with radar-bright material at latitudes south of 80°N are not uniformly distributed in longitude. Craters hosting radar-bright deposits show a strong preference for longitudes near 90°E longitude and, to a lesser extent, 270°E. The equatorial regions at longitudes of 90°E and 270°E are Mercury's "cold poles", where local noon occurs at aphelion because of Mercury's 3:2 spin-orbit resonance, and solar insolation is substantially less than at the corresponding "hot poles" at 0°E and 180°E because of Mercury's eccentric orbit, resulting in a maximum temperature at the equator of the "cold pole" that is 130 K less than that of the "hot pole" [*Vasavada et al*., 1999]. The preference for radar-bright deposits along Mercury's cold-pole longitudes was first noted by *Harmon et al*. [2001] and further supported by the findings of *Harmon* [2007] and *Harmon et al*. [2011], who suggested that the thermal environment of the lower-latitude cold-pole longitudes is more favorable for water ice than the corresponding hot-pole longitudes. Our mapping results in Figure 5 strengthen the observational evidence that the cold pole longitudes offer a more favorable thermal environment for radar-bright deposits.

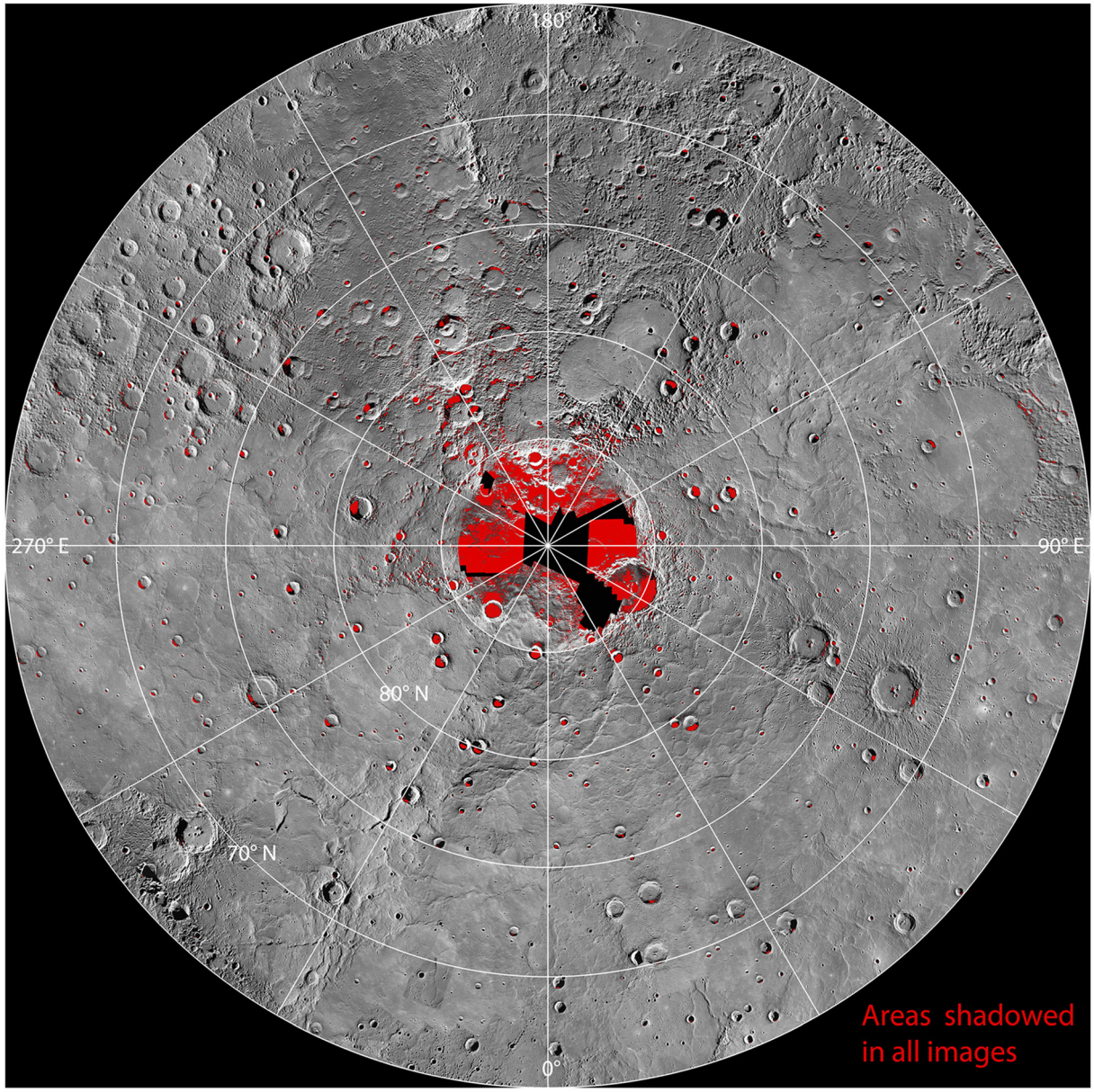

Figure 3. Areas shadowed in all WAC 750-nm-filter images from MESSENGER's primary orbital mission are shown in red on a polar stereographic mosaic of MESSENGER images. Image coverage, and consequently shadow mapping, is incomplete near Mercury's north pole.

3.2. Implications for Radar-Bright Materials

[16] Thermal models of Mercury's polar craters show that the temperatures within permanently shadowed regions depend strongly on the crater's size and latitude [*Paige et al.*, 1992; *Ingersoll et al.*, 1992; *Salvail and Fanale*, 1994]. More detailed models by *Vasavada et al.* [1999] yielded estimates for the maximum and average temperatures within shadowed craters with diameters of 100, 40, and 10 km on Mercury, which are summarized in Table 1. For craters 100 km in diameter and larger, the maximum temperature experienced by the coldest point within a permanently shadowed crater is <100 K for all latitudes poleward of ±80° [*Vasavada et al.*, 1999]. Moreover, the timescale to evaporate a deposit of water ice with a thickness of 1 m at a temperature of approximately 110 K is ~1 Gy [*Vasavada et al.*, 1999], so water-ice deposits in these craters would be thermally stable at the surface on geologic timescales. For Mercury's north polar region, there is one crater with a diameter >100 km located poleward of 80°N—the 112-km-diameter crater Prokofiev at 86°N, 64°E. According to the thermal modeling results of *Vasavada et al.* [1999], water ice could be thermally stable on the surface within permanently shadowed areas of Prokofiev.

[17] As detailed in the *Vasavada et al.* [1999] results in Table 1, craters with diameters ≥ 40 km and located north of 82°N could also have thermally stable water ice at the surface in the coldest permanently shadowed locations in their interiors. Four additional craters shown in Figure 5 meet those criteria, and two circular radar-bright features not mapped in Figure 5 because of a lack of image coverage

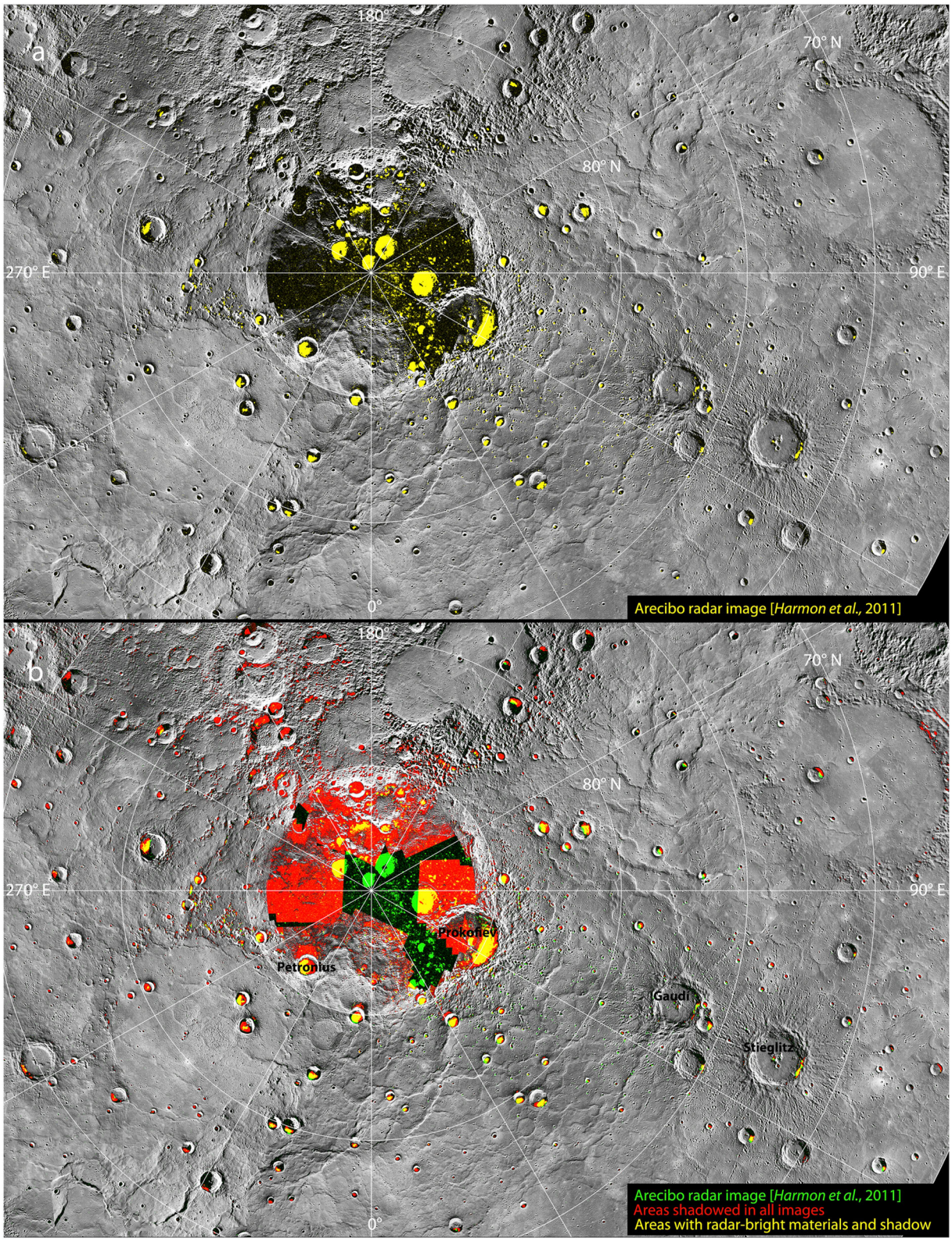

Figure 4. (a) Earth-based radar image from *Harmon et al*. [2011] in yellow, stretched to accentuate radar-bright locations, shows excellent qualitative correlation with cratered and other shadowed locations in the MESSENGER mosaic in polar stereographic projection. (b) A comparison between areas determined to be in persistent shadow (red) and the same Earth-based radar image (now in green). Locations where red persistently shadowed areas and green radar-bright deposits directly overlap are shown in yellow.

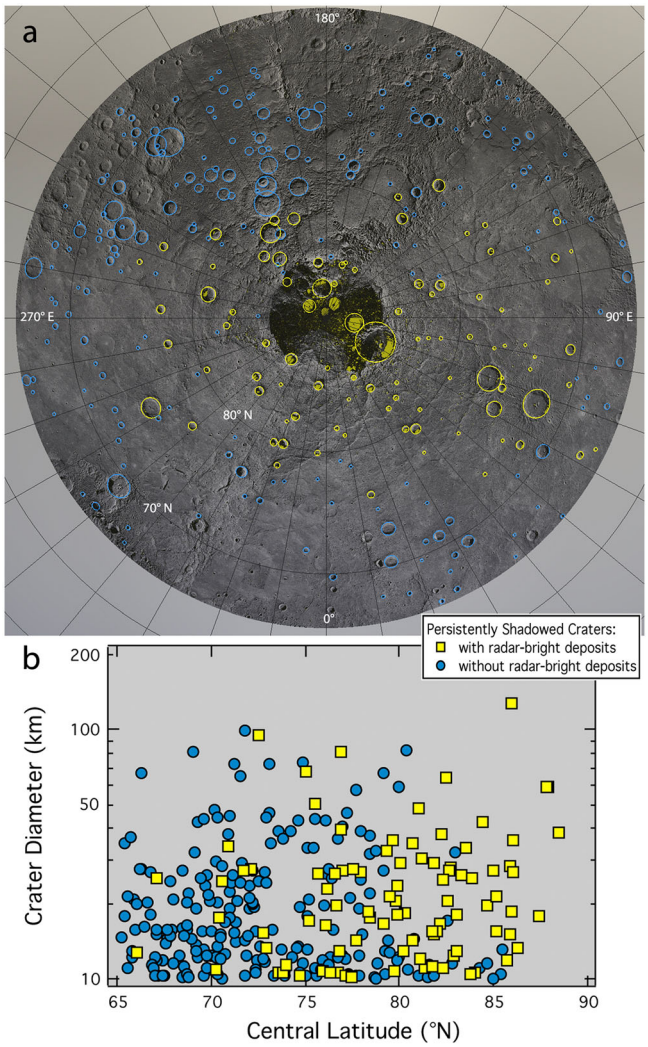

Figure 5. (a) Craters >10 km in diameter with interiors at least partially shadowed (Figure 3) are classified as either hosting radar-bright deposits (yellow) or not (blue) and (b) plotted as a function of their diameter and central latitude.

Table 1. Latitudes of Long-lived Water Ice Stability Within Permanently Shadowed Craters[a]

	10 km Bowl Shaped	40 km Flat-Floored	100 km Flat-Floored
Latitude range modeled	70°–90°	79°–90°	80°–90°
Latitude where maximum surface $T = 110$ K; long-lived surface ice is thermally stable.	None; max $T > 110$ K for all latitudes	82°	<80°
Latitude where average surface $T = 110$ K; long-lived ice with an insulating cover is thermally stable	88°	<79°	<80°

[a]All values from *Vasavada et al.* [1999], in particular their Figure 12 and text, and are for the coldest surface location in permanent shadow. T denotes temperature.

near the pole are potentially hosted by craters ≥40 km. For craters intermediate in diameter between 100 and 40 km, the latitude at which the surface temperature of the coldest shadowed location within the crater interior exceeds 110 K would also be intermediate between the two crater sizes modeled by *Vasavada et al.* [1999]. Additionally, *Vasavada et al.* [1999] specifically modeled the 35-km-diameter crater Petronius (86°N, 320°E) and found a surface temperature of the coldest shadowed location of <100 K. Overall, long-lived water ice would be thermally stable on the surface of many of the larger craters within ~10° of Mercury's pole in the coldest regions of permanent shadow.

[18] It should be noted that in any given crater, the coldest region in permanent shadow is a subarea of the larger permanently shadowed region. Thus, the total area that water ice could be thermally stable on the surface within each of these polar craters on Mercury requires evaluation on an individual basis. Using diameters and locations derived from Mariner 10 images and idealized crater shapes, *Vasavada et al.* [1999] conducted detailed thermal models of the temperature distributions within the shadowed areas of some craters hosting radar-bright deposits near Mercury's north pole. For example, *Vasavada et al.* [1999] found that roughly 20% of the permanently shaded region in Petronius has a surface temperature ≤110 K.

[19] In contrast, for craters located equatorward of 82°N and less than 40 km in diameter, the coldest surface locations in permanent shadow exceed 110 K. As seen on Figure 5, many craters that host radar-bright deposits meet these criteria, and surficial water ice would not be thermally stable on any surface inside these craters over a timescale of ~1 Gy. However, if the radar-bright deposits were covered by a thin, regolith layer, perhaps a few decimeters thick, then the peak temperature experienced by those deposits would be approximately equal to the average, rather than the maximum, surface temperature [*Vasavada et al.*, 1999]. Table 1 summarizes average surface temperature results from the models of *Vasavada et al.* [1999]. For many of the craters hosting radar-bright deposits plotted in Figure 5b, some insulating layer, such as a thin regolith cover, would enable water ice deposits at these locations to be stable for 1 Gy. A thin regolith cover has also been suggested on the basis of small differences in radar reflectivity and radar scattering parameters derived from the Arecibo 12.6-cm-wavelength S-band and Goldstone 3.5-cm-wavelength X-band data [*Butler et al.*, 1993; *Slade et al.*, 2004; *Harcke*, 2005; *Harmon et al.*, 2011]. Additionally, a thin regolith cover could provide a means to protect an ice deposit from erosion by interstellar Lyman-alpha radiation [*Morgan and Shemansky*, 1991; *Butler et al.*, 1993], an influence that is also relevant for permanently shadowed areas where long-lived water ice is thermally stable at the surface.

[20] The shadowed interiors of bowl-shaped simple craters experience considerably warmer temperatures than flatter-floored complex craters, due to increased indirect heating from scattering and infrared reradiation from crater walls [*Vasavada et al.*, 1999]. On Mercury, the transition with increasing diameter between simple and complex crater morphologies for primary craters occurs at a diameter of ~10 km [*Pike*, 1988; *Barnouin et al.*, 2012]. For primary bowl-shaped craters 10 km in diameter, *Vasavada et al.* [1999] calculated that the maximum surface temperature for the coldest shadowed location exceeded 110 K for all latitudes and that the average surface temperature was <110 K only when the crater was located within 2° of the

pole (Table 1). This result suggests that radar-bright deposits within primary simple craters ≤10 km in diameter south of 88°N cannot consist of water ice that has been present for ~1 Gy, even if buried beneath a thin insulating layer of regolith.

[21] Our mapping in Figure 5 is limited to craters greater than 10 km in diameter, but a comparison of the radar image of *Harmon et al*. [2011] with the MDIS base map images shows many craters <10 km in diameter that host radar-bright deposits. In particular, *Harmon et al*. [2011] noted "the remarkable profusion of small bright spots in the general region south of crater K" (now named Prokofiev); the Arecibo radar image for that region is shown in Figure 6a. Figure 6b reveals that many of the small radar-bright spots are associated with small secondary craters from Prokofiev or from other impacts in the area, such as the 81-km-diameter crater Gaudí at 77°N, 70°E. This region is located more than

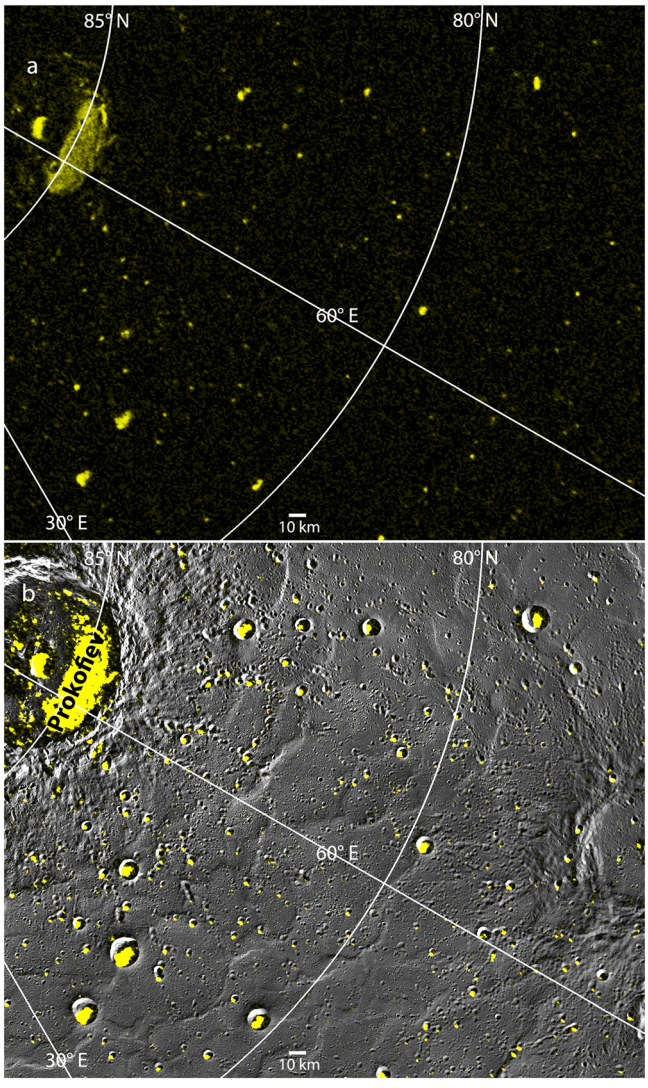

Figure 6. (a) Arecibo radar image (yellow) [*Harmon et al*., 2011] showing Prokofiev in the upper left corner and numerous small radar-bright features. (b) Comparison of the radar image with a mosaic of MESSENGER images reveals that the many small radar-bright features are associated with craters having diameters <10 km (scale bar at bottom of images).

2° from the pole, and thus the thermal modeling of *Vasavada et al*. [1999] suggests that long-lived water-ice would not be stable in these small, <10 km diameter craters for 1 Gy, even if insulated by a layer of regolith, if the craters resemble the morphology used in model. The region shown in Figure 6 is just one example area; small craters that host radar-bright deposits have also been identified in other regions near Mercury's north [*Harmon et al*., 2001] and south [*Chabot et al*., 2012] poles.

[22] The thermal modeling of *Vasavada et al*. [1999] necessarily was for idealized crater shapes, as spacecraft data were limited for Mercury prior to the MESSENGER mission. If these small craters are shallower than the idealized bowl shape, the thermal environment inside could potentially be more favorable to the retention of water ice on geologic timescales. Shallower craters would result in smaller areas of permanent shadow, but those shadowed areas would be colder, as sunlit crater walls would contribute less scattered and emitted energy to warming the shadowed region than would the steeper walls of a deeper crater [*Vasavada et al*., 1999]. *Vasavada et al*. [1999] concluded that in many ways the temperatures of permanently shadowed regions depend more strongly on crater shape than on latitude. On Mercury, a given size crater appears to have larger secondaries than on the Moon and Mars, with a substantial number of secondary craters having diameters ranging up to ~10 km [*Strom et al*., 2011]. In general, secondary craters exhibit lower depth/diameter ratios than expected for similarly sized primaries [*McEwen and Bierhaus*, 2006]. Thus, the interior of shallower secondary craters, such as shown in Figure 6, may provide a thermal environment more conducive to the presence of long-lived water ice than the idealized 10 km diameter simple crater shape used in the modeling of *Vasavada et al*. [1999].

[23] Additionally, topographic information obtained by MESSENGER's Mercury Laser Altimeter has revealed an extensive lowland at high northern latitudes, with a broad topographic rise within this otherwise low region [*Zuber et al*., 2012]. The surface shown in Figure 6 with Prokofiev and many small craters hosting radar-bright deposits is located in this lowland region, near the topographic rise, which could also potentially affect the thermal environment experienced inside the craters. As the Mercury Laser Altimeter coverage becomes more densely spaced and higher-resolution stereo imaging is acquired, detailed thermal modeling of these small craters that includes the crater's specific shape as well as the long-wavelength topography of Mercury could provide important insight into the specific thermal environment in these craters and, consequently, the timing of water ice emplacement on Mercury.

[24] Other locations that could pose a challenging thermal environment for water ice to be stable for ~1 Gy are craters hosting radar-bright deposits at lower latitudes. The thermal modeling of 40-km-diameter craters on Mercury by *Vasavada et al*. [1999] did not extend to latitudes equatorward of ±79°, whereas radar-bright features have been noted to extend to latitudes south of 70°N [*Harmon et al*., 2011]. As shown in Figure 5, there are 16 craters with diameters >10 km and central latitudes <75°N that host radar-bright deposits. Figure 7 shows the locations of the southernmost of these craters, extending to 66°N. As seen in Figure 7, the radar-bright deposits correlate with the

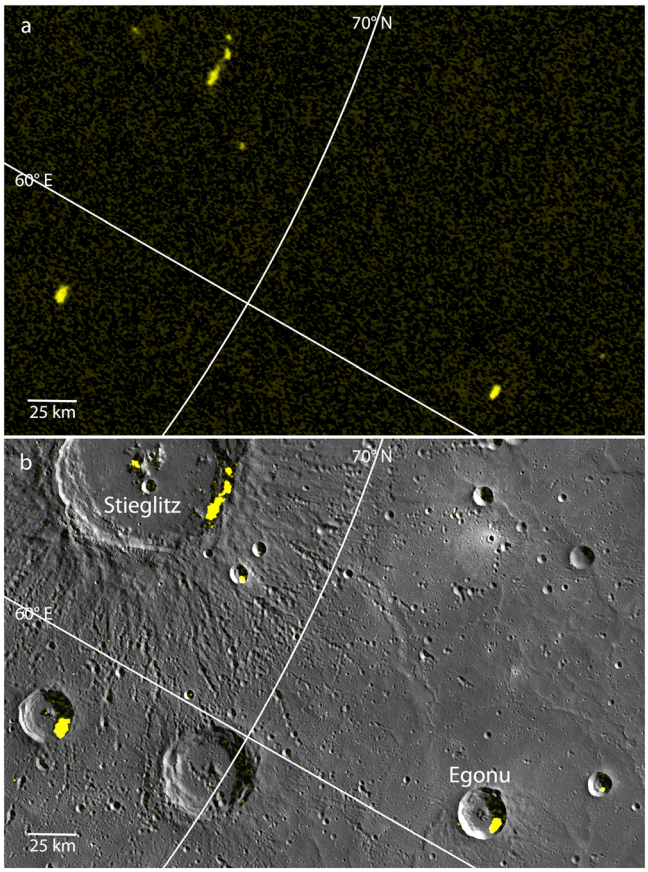

Figure 7. (a) Arecibo radar image (yellow) [*Harmon et al*., 2011] showing the lowest-latitude radar-bright features detected on Mercury. (b) Comparison of the radar image with a mosaic of MESSENGER images shows that the low-latitude radar-bright deposits are located at the shadowed southern walls of impact craters of a variety of sizes.

persistently shadowed, southern walls of impact craters, ranging in diameter from <10 km to 95 km. These lower-latitude craters are worthy of future detailed thermal modeling efforts, which should be possible with detailed topographic data to be obtained by MESSENGER.

[25] Cold-trapped elemental sulfur near Mercury's poles has been proposed as an alternative composition for the radar-bright polar deposits [*Sprague et al*., 1995]. Given some of the thermal environments that are challenging for the stability of water ice for ~1 Gy, sulfur has an attractive characteristic, as the evaporation rate of a 1 m thick deposit of elemental sulfur over 1 Gy corresponds to a surface temperature of ~220 K [*Vasavada et al*., 1999], considerably higher than the 110 K temperature for water ice. As detailed in Table 1, areas in permanent shadow within larger flat-floored craters experience maximum temperatures <220 K and bowl-shaped craters 10 km in diameter have average temperatures <220 K for all latitudes examined. Thus, radar-bright features associated with the small and lower-latitude craters, with examples shown in Figures 6 and 7, do not pose a thermal stability problem for sulfur to be present over a 1 Gy timeframe. However, sulfur's stability at higher temperature also has the implication that near the poles, a polar cap of sulfur is predicted. In particular, if sulfur were responsible for the radar-bright features on Mercury, a sulfur polar cap with a radius of approximately 1° in latitude is predicted [*Butler*, 1997; *Vasavada et al*., 1999]; no such polar cap has been detected by any observations of Mercury's polar regions. Additionally, there is no quantitative study that shows that a layer of sulfur would create the high reflectivity and circular polarization ratio of the observed radar-bright features on Mercury, along the lines of that modeled by *Black et al*. [2001] for water ice on the Galilean satellites.

[26] Another alternative for the nature of Mercury's radar-bright materials was proposed by *Starukhina* [2001], who suggested that Mercury's high-radar-backscatter signals originate from altered dielectric properties of silicates at very low temperatures rather than from cold-trapped volatiles such as water ice or sulfur. That Mercury's radar-bright deposits are observed to correspond with persistently shadowed areas is consistent with locations where silicates would experience the lowest temperatures on Mercury, and thus this observation alone cannot distinguish between the cold silicate hypothesis of *Starukhina* [2001] and the cold-trapped volatiles proposals. However, shadowed regions at the lunar poles are considerably colder than those at Mercury [*Paige et al*., 2010], yet radar observations of the Moon do not show any spatial correlation between permanently shadowed areas and features with high circular polarization ratios [*Campbell and Campbell*, 2006; *Campbell et al*., 2006]. Similarly, recent orbital radar observations with the Miniature Radio Frequency (Mini-RF) instrument on the Lunar Reconnaissance Orbiter spacecraft do not show a correlation between high-radar-backscatter signals and shadowed regions [*Neish et al*., 2011; *Thomson et al*., 2012]. The silicate composition of Mercury and the Moon differ, but the lack of strong radar-backscatter signal in the very cold shadowed lunar polar regions requires an explanation if cold silicates are responsible for the radar-bright materials on Mercury but do not produce the same radar signature on the Moon.

[27] The observation that nearly every persistently shadowed crater >10 km in diameter within 10° of Mercury's north pole hosts a radar-bright deposit suggests that either the source of the radar-bright material or the migration of the radar-bright material results in a global distribution that reaches all available cold traps. Craters hosting radar-bright deposits near Mercury's north pole do not show a localized distribution other than that related to the thermal environment. That there is not a population of shadowed craters with a thermally favorable environment that lack radar-bright deposits means that no limit can be placed on the youngest possible age for the emplacement of the radar-bright material on the basis solely of the geographic distribution of host craters. In contrast, the presence of numerous small craters that host radar-bright material may imply that water ice was emplaced relatively recently in Mercury's history or there is an active mechanism for resupply. That water ice near Mercury's poles is relatively recently emplaced has been suggested by *Crider and Killen* [2005], on the basis of models for the burial of ice on Mercury through regolith emplacement for a range of initial ice thicknesses and regolith covers. *Crider and Killen* [2005] concluded that if the radar-bright deposits on Mercury are relatively pure water ice that are currently covered by 20 cm of regolith, then the

water ice must have been emplaced <50 My ago. Detailed thermal modeling of small craters that host radar-bright deposits will be crucial for addressing this important issue regarding the timing, source, and nature of Mercury's radar-bright materials.

4. Conclusions

[28] Images from MESSENGER's one-year primary mission enable many craters that host radar-bright deposits at Mercury's north polar region to be identified for the first time. By mapping regions persistently shadowed in all images, we may make the following conclusions: (1) Radar-bright features near Mercury's north pole are associated with locations persistently shadowed in MESSENGER images, consistent with the hypothesis that the radar-bright material consists of cold-trapped volatiles such as water ice. (2) Nearly all craters >10 km in diameter within 10° of Mercury's north pole host radar-bright material, suggesting a source or migration process for the radar-bright material that allows it to reach all available cold traps. (3) Craters located at lower latitudes, more than ~10° from the pole, show a preference for being hosted in persistently shadowed regions of craters located near Mercury's cold-pole longitudes of 90°E and 270°E. (4) There are several craters in Mercury's north polar region with large (≥40 km) diameters located at high latitudes (within ~8° of the pole) that have the potential to contain long-lived water ice on the surface in permanently shadowed regions. (5) Many radar-bright features are located in craters <40 km in diameter and more than ~8° from the pole and thus require a thin insulating cover of regolith or other material if such features are the result of long-lived water ice. (6) Numerous radar-bright features are associated with small (<10 km diameter) or lower-latitude craters, which may be challenging thermal environments for water ice to be stable for ~1 Gy. Understanding the thermal environment inside these small and lower-latitude craters, together with acquired and ongoing laser altimetry, neutron spectrometry, and high-resolution stereo imaging by the MESSENGER spacecraft, could provide crucial constraints on the nature, source, and timing of emplacement of the radar-bright materials.

[29] **Acknowledgments.** We thank Bruce A. Campbell and an anonymous reviewer for comments that improved this manuscript, and Mark Wieczorek for editorial handling. The MESSENGER project is supported by the NASA Discovery Program under contracts NAS5-97271 to The Johns Hopkins University Applied Physics Laboratory and NASW-00002 to the Carnegie Institution of Washington. Support from a MESSENGER Participating Scientist grant to D. T. B. is also appreciated.

References

Barnouin, O. S., M. T. Zuber, D. E. Smith, G. A. Neumann, R. R. Herrick, J. E. Chappelow, S. L. Murchie, and L. M. Prockter (2012), The morphology of craters on Mercury: Results from MESSENGER flybys, *Icarus*, *219*, 414–427.

Becker, K. J., L. A. Weller, K. L. Edmundson, T. L. Becker, M. S. Robinson, A. C. Enns, and S. C. Solomon (2012), Global controlled mosaic of Mercury from MESSENGER orbital images, *Lunar Planet. Sci.*, *43*, abstract 2654.

Black, G. J., D. B. Campbell, and P. D. Nicholson (2001), Icy Galilean satellites: Modeling radar reflectivities as coherent backscatter effect, *Icarus*, *151*, 167–180.

Bussey, D. B. J., P. D. Spudis, and M. S. Robinson (1999), Illumination conditions at the lunar south pole, *Geophys. Res. Lett.*, *26*, 1187–1190.

Bussey, D. B. J., K. E. Fristad, P. M. Schenk, M. S. Robinson, and P. D. Spudis (2005), Constant illumination at the lunar north pole, *Nature*, *434*, 842.

Butler, B. J. (1997), The migration of volatiles on the surfaces of Mercury and the Moon, *J. Geophys. Res.*, *102*, 19,283–19,291.

Butler, B. J., D. O. Muhleman, and M. A. Slade (1993), Mercury: Full–disk radar images and the detection and stability of ice at the north pole, *J. Geophys. Res.*, *98*, 15,003–15,023.

Campbell, B. A., and D. B. Campbell (2006), Regolith properties in the south polar region of the Moon from 70-cm radar polarimetry, *Icarus*, *180*, 1–7.

Campbell, D. B., B. A. Campbell, L. M. Carter, J.-L. Margot, and N. J. S. Stacy (2006), No evidence for thick deposits of ice at the lunar south pole, *Nature*, *443*, 835–837.

Chabot, N. L., C. M. Ernst, B. W. Denevi, J. K. Harmon, S. L. Murchie, D. T. Blewett, S. C. Solomon, and E. D. Zhong (2012), Areas of permanent shadow in Mercury's south polar region ascertained by MESSENGER orbital imaging, *Geophys. Res. Lett.*, *39*, L09204, doi:10.1029/2012GL051526.

Crider, D., and R. M. Killen (2005), Burial rate of Mercury's polar volatile deposits, *Geophys. Res. Lett.*, *32*, L12201, doi:10.1029/2005GL022689.

Davies, M. E., S. E. Dwornik, D. E. Gault, and R. G. Strom (1978), Atlas of Mercury, Special Publication SP–423, National Aeronautics and Space Administration, Washington, D.C., 128 pp.

Harcke, L. J. (2005), Radar imaging of solar system ices, Ph.D. thesis, Stanford University, Stanford, Calif., 201 pp.

Harmon, J. K. (2007), Radar imaging of Mercury. *Space Sci. Rev.*, *132*, 307–349.

Harmon, J. K., and M. A. Slade (1992), Radar mapping of Mercury: Full–disk images and polar anomalies, *Science*, *258*, 640–643.

Harmon, J. K., M. A. Slade, R. A. Vélez, A. Crespo, M. J. Dryer, and J. M. Johnson (1994), Radar mapping of Mercury's polar anomalies, *Nature*, *369*, 213–215.

Harmon, J. K., P. J. Perillat, and M. A. Slade (2001), High–resolution radar imaging of Mercury's north pole, *Icarus*, *149*, 1–15.

Harmon, J. K., M. A. Slade, and M. S. Rice (2011), Radar imagery of Mercury's putative polar ice: 1999–2005 Arecibo results, *Icarus*, *211*, 37–50.

Hawkins, S. E., III, et al. (2007), The Mercury Dual Imaging System on the MESSENGER spacecraft. *Space Sci. Rev.*, *131*, 247–338.

Ingersoll, A. P., T. Svitek, and B. C. Murray (1992), Stability of polar frosts in spherical bowl–shaped craters on Moon Mercury, and Mars, *Icarus*, *100*, 40–47.

Margot, J.-L., S. J. Peale, S. C. Solomon, S. A. Hauck II, F. D. Ghigo, R. F. Jurgens, M. Yseboodt, J. D. Giorgini, S. Padovan, and D. B. Campbell (2012), Mercury's moment of inertia from spin and gravity data, *J. Geophys. Res.*, *117*, E00L09, doi:10.1029/2012JE004161.

Mazarico, E., G. A. Neumann, D. E. Smith, M. T. Zuber, and M. H. Torrence (2011), Illumination conditions of the lunar polar regions using LOLA topography, *Icarus*, *211*, 1066–1081.

McEwen, A. S., and E. B. Bierhaus (2006), The importance of secondary cratering to age constraints on planetary surfaces, *Annu. Rev. Earth Planet. Sci.*, *34*, 535–567.

Morgan, T. H., and D. E. Shemansky (1991), Limits to the lunar atmosphere, *J. Geophys. Res.*, *96*, 1351–1367.

Neish, C. D., D. B. J. Bussey, P. Spudis, W. Marshall, B. J. Thomson, G. W. Patterson, and L. M. Carter (2011), The nature of lunar volatiles as revealed by Mini–RF observations of the LCROSS impact site, *J. Geophys. Res.*, *116*, E01005, doi:10.1029/2010JE003647.

Paige, D. A., S. E. Wood, and A. R. Vasavada (1992), The thermal stability of water ice at the poles of Mercury, *Science*, *258*, 643–646.

Paige, D. A., et al. (2010), Diviner lunar radiometer observations of cold traps in the Moon's south polar region, *Science*, *330*, 479–482.

Pike, R. J. (1988), Geomorphology of impact craters on Mercury, in Mercury, edited by F. Vilas, C. R. Chapman, and M. S. Matthews, University of Arizona Press, Tucson, Ariz., pp. 165–273.

Robinson M. S., M. E. Davies, T. R. Colvin, and K. Edwards (1999), A revised control network for Mercury, *J. Geophys. Res.*, *104*, 30,847–30,852.

Salvail, J. R., and F. P. Fanale (1994), Near–surface ice on Mercury and the Moon: A topographic thermal model, *Icarus*, *111*, 441–455.

Slade, M. A., B. J. Butler, and D. O. Muhleman (1992), Mercury radar imaging: Evidence for polar ice, *Science*, *258*, 635–640.

Slade, M. A., L. J. Harcke, R. F. Jurgens, and H. A. Zebker (2001), Mercury's north and south polar regions: Goldstone radar imaging at 3.5–cm wavelength, *Bull. Amer. Astron. Soc.*, *33*, 1026.

Slade M., J. Harmon, L. Harcke, and R. Jurgens (2004), 3.5–cm radar observations of polar regions of Mercury using Goldstone to Arecibo configuration, *Abstracts*, *35th COSPAR Scientific Assembly 2004*, abstract COSPAR04–A–01154, CD–ROM.

Solomon, S. C., R. L. McNutt Jr., R. E. Gold, and D. L. Domingue (2007), MESSENGER mission overview, *Space Sci. Rev.*, *131*, 3–39.

Speyerer, E. J., and M. S. Robinson (2011), Analysis of highly illuminated zones near the lunar south pole, *Lunar Planet. Sci.*, *42*, abstract 2540.

Sprague, A. L., D. M. Hunten, and K. Lodders (1995), Sulfur at Mercury, elemental at the poles and sulfides in the regolith, *Icarus*, *118*, 211–215.

Starukhina, L. (2001), Water detection on atmosphereless celestial bodies: Alternative explanations of the observations, *J. Geophys. Res.*, *106*, 14,701–14,710.

Strom, R. G., M. E. Banks, C. R. Chapman, C. I. Fassett, J. A. Forde, J. W. Head III, W. J. Merline, L. M. Prockter, and S. C. Solomon (2011), Mercury crater statistics from MESSENGER flybys: Implications for stratigraphy and resurfacing history, *Planet. Space Sci.*, *59*, 1960–1967.

Thomson, B. J., et al. (2012), An upper limit for ice in Shackleton crater as revealed by LRO Mini–RF orbital radar, *Geophys. Res. Lett.*, *39*, L14201, doi:10.1029/2012GL052119.

Vasavada, A. R., D. A. Paige, and S. E. Wood (1999), Near–surface temperatures on Mercury and the Moon and the stability of polar ice deposits, *Icarus*, *141*, 179–193.

Zuber, M. T., et al. (2012), Topography of the northern hemisphere of Mercury from MESSENGER laser altimetry, *Science*, *336*, 217–220.